Numerical Heat Transfer, Part B: Fundamentals: An International Journal of Computation and Methodology
Publication details, including instructions for authors and subscription information:
http://www.tandfonline.com/loi/unhb20

Use of Characteristic-Based Flux Limiters in a Pressure-Based Unstructured-Grid Algorithm Incorporating High-Resolution Schemes

Yeng-Yung Tsui [a] & Tian-Cherng Wu [a]
[a] Department of Mechanical Engineering , National Chiao Tung University , Hsinchu, Taiwan, Republic of China
Published online: 22 Dec 2008.

To cite this article: Yeng-Yung Tsui & Tian-Cherng Wu (2009) Use of Characteristic-Based Flux Limiters in a Pressure-Based Unstructured-Grid Algorithm Incorporating High-Resolution Schemes, Numerical Heat Transfer, Part B: Fundamentals: An International Journal of Computation and Methodology, 55:1, 14-34, DOI: 10.1080/10407790802605091

To link to this article: http://dx.doi.org/10.1080/10407790802605091

Numerical Heat Transfer, Part B, 55: 14–34, 2009

ISSN: 1040-7790 print/1521-0626 online
DOI: 10.1080/10407790802605091

Taylor & Francis
Taylor & Francis Group

USE OF CHARACTERISTIC-BASED FLUX LIMITERS IN A PRESSURE-BASED UNSTRUCTURED-GRID ALGORITHM INCORPORATING HIGH-RESOLUTION SCHEMES

Yeng-Yung Tsui and Tian-Cherng Wu
Department of Mechanical Engineering, National Chiao Tung University, Hsinchu, Taiwan, Republic of China

A pressure-based procedure to solve problems ranging from incompressible to highly compressible flows is described. The method adopts the fully conservative finite-volume approach, for which the meshes can be of any topology. To handle the sharp change of the gradient in the regions near the shock or the solid wall, the convective flux is limited using high-resolution schemes such as the total variation diminishing (TVD) or the normalized variable diagram (NVD) scheme. The flux limiters are determined from the characteristic variables instead of the commonly used primitive or conservative variables. To enhance solution accuracy, the gradient is calculated using a linear reconstruction approach. The method is assessed and validated via testing on a number of flow problems, including inviscid flows through a convergent-divergent nozzle, inviscid and viscous flows past an airfoil, and viscous flows through a double-throat nozzle.

INTRODUCTION

For convection-dominated flows, the approximation to the advection term is of great importance to the accuracy and stability of numerical solutions. It was recognized that for high-order linear schemes the coefficients of the difference equation may become negative and, thus, tend to introduce spurious oscillations in the solution where the gradients change sharply [1]. To remedy this problem, Spalding [2] proposed a hybrid scheme which uses the second-order central difference scheme for the absolute value of the cell Peclet number less than 2 and switches to the first-order upwind difference scheme elsewhere. In the flux-corrected transport method of Borris and Brook [3], the solution is obtained in a predictor-corrector manner. In the predictor step, a low-order diffusive scheme is used to obtain a positive, monotonic solution. It is followed by a corrector step in which a certain amount of diffusion flux, which may have been excessive, is removed in a way that no new extrema will be created.

Received 17 September 2008; accepted 17 October 2008.
The work was supported by the Science Research Council of the Republic of China under Contract NSC 93-2212-E-009-012.
Address correspondence to Yeng-Yung Tsui, Department of Mechanical Engineering, National Chiao Tung University, 1001 Ta-Hsueh Road, Hsinchu 300, Taiwan, Republic of China. E-mail: yytsui@mail.nctu.edu.tw

NOMENCLATURE

A_C, A_P	coefficients of difference equation
B_C	coefficient defined by Eq. (31)
$\vec{d}$	a vector defined in the direction of $\vec{\delta}_{PC}$
D	pressure coefficient in difference equation
e	internal energy
F_f^C	convective flux
F_f^D	diffusive flux
k	conduction coefficient
K	inverse of the square of the speed of sound
$\dot{m}$	mass flux
P	pressure
P_o	total pressure
P'	pressure correction
r	ratio of two consecutive gradients
R	gas constant
S	source term of difference equation
$\vec{S}_f$	surface vector of cell face
S_ϕ	source term of transport equation
T	temperature
$\mathbf{T}$	Jacobian matrix
T_o	total temperature
$\vec{V}$	flow velocity vector
V_∞	velocity at infinity
γ	ratio of specific heats
γ_f	flux limiter
Γ	diffusion coefficient
$\vec{\delta}_{PC}$	distance vector from node P to node C
$\vec{\delta}_{BD}$	distance vector from node B to node D
ΔV	cell volume
Δt	time interval
μ	dynamic viscosity
ρ	density
τ_{ij}	viscous stress tensor
ϕ	transport variable
ϕ_B, ϕ_D, ϕ_U	values of ϕ at the upstream, downstream, and far upstream nodes
φ	characteristic variable
$\varphi_B, \varphi_D, \varphi_U$	values of φ at the upstream, downstream, and far upstream nodes

Subscripts

B	a node upstream of the considered face
C	neighboring cell node
D	a node downstream of the considered face
f	a face of the control volume surface
P	primary cell node
U	a node far upstream of the considered face

Superscripts

o	old-time-level value
$*$	prevailing value
$'$	correction

In hyperbolic systems, the characteristic speeds (or the eigenvalues) are of mixed signs for subsonic flows. Information can be propagated both upstream and downstream along the characteristics. In supersonic flows, information can be transmitted only in the downstream direction because the characteristic speeds are of the same sign. To reflect this fact, Beam and Warming [4] adopted a hybrid strategy which switches automatically from central difference schemes to upwind difference schemes whenever the eigenvalues change from mixed sign to all positive. Later, this inspires the development of the flux-vector splitting method [5, 6].

In past years, a lot of effort has been devoted to developing nonlinear schemes by which high-order-accurate and bounded solutions are obtained. One of these is the total variation diminishing (TVD) type of scheme introduced by Harten [7]. These schemes usually involve limiters to control convective flux such that the solution satisfies the total variation diminishing conditions [8, 9]. The limiters are usually expressed as a function of the gradient ratio. These TVD schemes are mostly found in density-based methods to capture shocks in transonic and supersonic flows.

Another approach was later introduced by Leonard [10] in the form of a normalized variable diagram (NVD). After the variables have been normalized, the face value is related to the value only at the upwind node. Solution monotonicity is achieved by satisfying the convection boundedness criterion of Gaskell and Lau [11]. It was shown by Leonard [12] that a number of TVD flux limiters can be reinterpreted in the NVD, allowing for easier understanding of their characteristics. This kind of scheme is mostly adopted in the pressure-based methods.

The nonlinear schemes usually switch between different linear schemes according to the flux limiter such as that used in the TVD schemes or the normalized upwind value in the NVD schemes. In order to construct the flux-limiting function to find the face flux, it is a natural choice to use either the primitive variables or the conservative variables, because they are the dependent variables to formulate the governing equations. Alternatively, Mulder and Van Leer [13] used characteristic variables in their averaging procedure, which employs the Van Albada limiting function [14] to solve a one-dimensional flow problem with isothermal gas along an almost circular path through the stellar gravitational field of a rotating two-armed spiral galaxy. It was shown that the solution is a notch better in the regions where the flow is smooth, but with the convergence improved significantly. Lin and Chieng [15] incorporated a number of high-order schemes in the form of NVD. It is apparent from the one-dimensional shock tube flow that the oscillations around the expansion waves and the shock waves are reduced when the indicator of the switching procedure is changed from primitive or conservative variables to the characteristic variables. Also shown is less iteration required in the oblique-shock step flow. Similar conclusions have been addressed by Dadone and Grossman [16], who adopted the MINMOD limiter in their rotated upwind scheme. The use of a characteristic-based limiter can also be found in the work of Pan and Cheng [17], in which the limiter of Barth and Jespersen [18] was utilized.

In the articles cited above, the solutions of the flow problems were obtained with density-based methods. Implementation of characteristic-based limiters into the pressure-based methods is scarce. Kobayashi and Pereira [19] incorporated the characteristic interpolation practice into Roe's approximate Riemann solver [20, 21] for calculation of the convective flux. This was followed by a predictor-corrector procedure to treat the coupling between the momentum equations and the continuity equation, just as in the SIMPLE algorithm. In the work of Issa and Javareshkian [22], the convective flux was formulated in the form proposed by Yee et al. [23]. The MINMOD limiter was then used.

In the above studies, the numerical methods were constructed within the framework of structured grids. The only exception is that of Pan and Cheng [17], in which unstructured triangular meshes were utilized. On unstructured grids, information at the nodes far away from the considered face is difficult to obtain, and the far upstream nodes cannot be identified for nonquadrilateral grids. The limiting process used by Pan and Cheng was based on a piecewise-linear reconstruction of cell-averaged solution data while ensuring that no value in the cell greater than the surrounding neighbor values was created [18]. In a recent study by the present authors [24], a methodology utilizing a pressure-based unstructured grid algorithm was developed for all-speed flows. In this work, the far-upstream node value, as required in the limiting processes of the TVD and NVD schemes, can be estimated from a linear

reconstruction. Therefore, a vast number of TVD and NVD schemes can easily be implemented. In this study, this method is extended to incorporate characteristic variables as the basis for the limiting indicators.

HYPERBOLIC SYSTEMS

In two dimensions, the conservation laws for the inviscid flow in quasi-linear form can be written as

$$\frac{\partial U}{\partial t} + A\frac{\partial U}{\partial x} + B\frac{\partial U}{\partial y} = 0 \tag{1}$$

where

$$U = \begin{bmatrix} \rho \\ u \\ v \\ e \end{bmatrix} \quad A = \begin{bmatrix} u & \rho & 0 & 0 \\ (\gamma-1)e/\rho & u & 0 & \gamma-1 \\ 0 & 0 & u & 0 \\ 0 & p/\rho & 0 & u \end{bmatrix} \quad B = \begin{bmatrix} v & \rho & 0 & 0 \\ 0 & v & 0 & 0 \\ (\gamma-1)e/\rho & 0 & v & \gamma-1 \\ 0 & 0 & p/\rho & v \end{bmatrix} \tag{2}$$

Here primitive variables (density ρ, velocities u and v, and internal energy e) are used as dependent variables.

The equation of state is

$$P = (\gamma - 1)\rho e \tag{3}$$

where γ is the ratio of specific heats. Define a matrix $\mathbf{P}$

$$\mathbf{P} = k_1 A + k_2 B \tag{4}$$

where k_1 and k_2 are arbitrary real numbers. The system is hyperbolic because there exists a similarity transformation such that

$$\mathbf{T}^{-1}\mathbf{P}\mathbf{T} = \Lambda \tag{5}$$

Here Λ is a diagonal matrix formed by the eigenvalues of $\mathbf{P}$,

$$\lambda_{1,2} = k_1 u + k_2 v \quad \lambda_{3,4} = \lambda_1 \pm kc \quad k = \sqrt{k_1^2 + k_2^2} \tag{6}$$

where c is the speed of sound. The matrices $\mathbf{T}$ and $\mathbf{T}^{-1}$ are given by

$$\mathbf{T} = \begin{bmatrix} 1 & 0 & \rho/c & \rho/c \\ 0 & k_2 & k_1/k & -k_1/k \\ 0 & -k_1 & k_2/k & -k_2/k \\ -c^2/\gamma(\gamma-1)\rho & 0 & c/\gamma & c/\gamma \end{bmatrix}$$
$$\mathbf{T}^{-1} = \begin{bmatrix} (\gamma-1)/\gamma & 0 & 0 & -(\gamma-1)\rho/c^2 \\ 0 & k_2/k^2 & -k/k^2 & 0 \\ c/2\gamma\rho & k_1/2k & k_2/2k & (\gamma-1)/2c \\ c/2\gamma\rho & -k_1/2k & -k_2/2k & (\gamma-1)/2c \end{bmatrix} \tag{7}$$

The jth column of $\mathbf{T}$ is a right eigenvector of $\mathbf{P}$, corresponding to the eigenvalue λ_j.

GOVERNING EQUATIONS

The basic equations describing the conservation of mass, momentum, and energy for viscous flows can be expressed in tensor notation as

$$\frac{\partial \rho}{\partial t} + \frac{\partial}{\partial x_j}(\rho v_j) = 0 \tag{8}$$

$$\frac{\partial \rho v_i}{\partial t} + \frac{\partial}{\partial x_j}(\rho v_j v_i) = -\frac{\partial p}{\partial x_i} + \frac{\partial \tau_{ij}}{\partial x_j} \tag{9}$$

$$\frac{\partial \rho e}{\partial t} + \frac{\partial}{\partial x_j}(\rho v_j e) = \frac{\partial}{\partial x_j}\left(k\frac{\partial T}{\partial x_j}\right) - p\frac{\partial v_j}{\partial x_j} + \tau_{ij}\frac{\partial v_j}{\partial x_i} \tag{10}$$

where k is the heat conduction coefficient and τ_{ij} is the viscous stress tensor:

$$\tau_{ij} = -\frac{2}{3}\mu\frac{\partial v_k}{\partial x_k}\delta_{ij} + 2\mu\frac{\partial v_j}{\partial x_i} \tag{11}$$

The mathematic problem is closed by the equation of state,

$$P = \rho RT \tag{12}$$

DISCRETIZATION

The cells (or control volumes) used to construct an unstructured grid can be of arbitrary topology, which renders the finite-volume method more suitable for discretization. The governing equations are first integrated over a control volume. This is followed by applying the divergence theorem such that the volume integrals of the convection and diffusion terms are transformed into surface integrals. For a variable ϕ, the equation can be cast into the following general form:

$$\int_{CV} \frac{\partial \rho\phi}{\partial t} dV + \int_{CS} (\rho\vec{\mathbf{V}}\phi)\, d\vec{S} = \int_{CS} \Gamma\nabla\phi\, d\vec{S} + \int_{CV} S_\phi\, dV \tag{13}$$

where Γ stands for the diffusion coefficient and S_ϕ represents all the terms not appearing in the equation, which are lumped into a source.

The above equation can be discretized by the following approximation:

$$[(\rho\phi)_P - (\rho\phi)_P^o]\frac{\Delta V}{\Delta t} + \sum \dot{m}_f \phi_f = \sum \Gamma_f \nabla\phi_f \bullet \vec{S}_f + S_\phi\, \Delta V \tag{14}$$

Here the fully implicit scheme is employed for the time differencing. The subscript f denotes the surface faces of the considered cell P, and the summation is taken over all the surrounding faces. In the equation, $\dot{m}_f$ is the mass flux through the face and $\vec{S}_f$ is the surface vector of the face. The second term on the left-hand side represents the total convective fluxes across the control-volume surface, and the first term on

the right-hand side is the total diffusive fluxes. These two transport fluxes together with the mass fluxes require further approximation.

Diffusive Fluxes

Consider a cell P and a neighbor cell C with a common face f as shown in Figure 1. The diffusive flux F_f^D across the face f is approximated by [25]

$$F_f^D = \frac{\Gamma|\vec{S}_f|^2}{\vec{\delta}_{PC} \bullet \vec{S}_f}(\phi_C - \phi_P) + \Gamma\overline{\nabla\phi_f} \bullet (\vec{S}_f - \vec{d}) \tag{15}$$

where $\vec{\delta}_{PC}$ is the distance vector connecting the node P and the node C, and $\vec{d}$ is defined as

$$\vec{d} \equiv \frac{|\vec{S}_f|^2}{\vec{\delta}_{PC} \bullet \vec{S}_f}\vec{\delta}_{PC} \tag{16}$$

The overbar on the face gradient indicates that it is obtained via interpolation from the two nodes P and C. The first part of the expression represents the derivative along the local coordinate $\vec{\delta}_{PC}$ and the second part stands for the cross-derivative arising in nonorthogonal grids when $\vec{\delta}_{PC}$ is not perpendicular to the face f.

Convective Fluxes

For the convective flux, the face value ϕ_f is estimated using neighboring nodal values as

$$\phi_f = \phi_B + \frac{\gamma_f(r)}{2}(\phi_D - \phi_B) \tag{17}$$

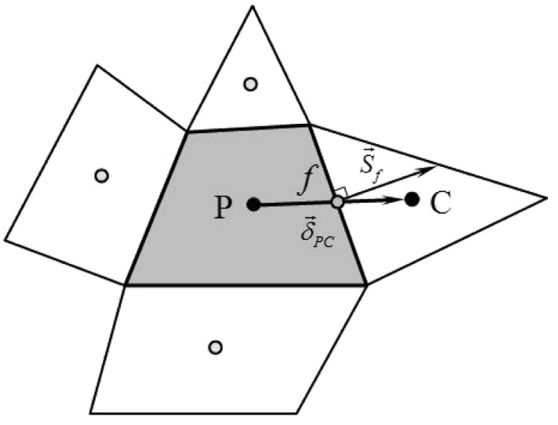

Figure 1. Illustration of a typical control volume with neighboring cells.

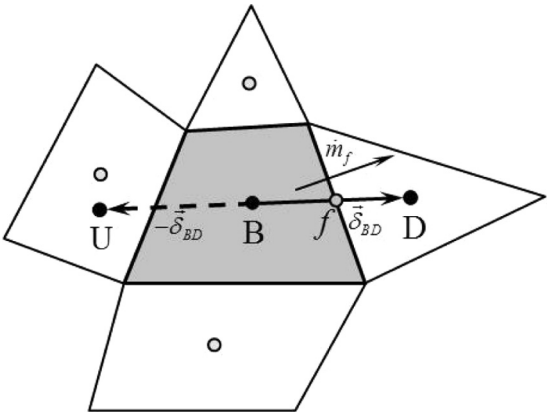

Figure 2. Illustration of calculation of the far upstream value ϕ_u.

where ϕ_B denotes the value at an upstream node B and ϕ_D the value at a node D downstream of the face f, as shown in Figure 2. In the expression, the second term represents the antidiffusion correction to the upwind difference scheme. For $\gamma_f = 0$, 1, 2, it simply represents the upwind, central, and downwind difference schemes, respectively. The coefficient $\gamma_f(r)$ stands for a flux-limiting function depending on the ratio of gradients r defined by

$$r = \frac{\phi_B - \phi_U}{\phi_D - \phi_B} \tag{18}$$

where ϕ_U is the value at a node far upstream of the face f. It was shown by Sweby [8] that the limiter must lie in the range between 0 and 2 to satisfy the TVD conditions.

In determination of the gradient ratio r, the far upwind node value ϕ_U needs to be known. We assume that the solution ϕ is distributed in a piecewise-linear sense. Let the node U be placed at a location $-\vec{\delta}_{BD}$ away from node B (see Figure 2). Then the value ϕ_U can be estimated by

$$\phi_U = \phi_D - 2\nabla\phi_B \bullet \vec{\delta}_{BD} \tag{19}$$

Substituting this into Eq. (18) leads to

$$r = \frac{2\nabla\phi_B \bullet \vec{\delta}_{BD}}{\phi_D - \phi_B} - 1 \tag{20}$$

The above formulations can also be expressed in terms of normalized variables, as was done by Leonard [10].

$$\tilde{\phi} = \frac{\phi - \phi_U}{\phi_D - \phi_U} \tag{21}$$

Thus,

$$r = \frac{\tilde{\phi}_B}{1 - \tilde{\phi}_B} \tag{22}$$

where

$$\tilde{\phi}_B = 1 - \frac{\phi_D - \phi_B}{2\nabla\phi_B \bullet \vec{\delta}_{BD}} \tag{23}$$

There are a vast number of TVD and NVD schemes to be used [24]. In the following, the SUPERBEE limiter of Roe [26] and that of Van Albada [27] are chosen in our calculations.

$$\text{SUPERBEE} \quad \gamma_f(r) = \max\{0, \min(r,\ 2), \min(2r,\ 1)\} \tag{24}$$

$$\text{Van Albada} \quad \gamma_f(r) = \begin{cases} \frac{(r^2+r)}{(r^2+1)} & r \geq 0 \\ 0 & r < 0 \end{cases} \tag{25}$$

These schemes can also be expressed in the normalized variable formulation (NVF) as

$$\text{SUPERBEE} \quad \begin{cases} \tilde{\phi}_f = 2\tilde{\phi}_B & 0 < \tilde{\phi}_B \leq \frac{1}{3} \\ \tilde{\phi}_f = \frac{1}{2}(\tilde{\phi}_B + 1) & \frac{1}{3} < \tilde{\phi}_B \leq \frac{1}{2} \\ \tilde{\phi}_f = \frac{3}{2}\tilde{\phi}_B & \frac{1}{2} < \tilde{\phi}_B \leq \frac{2}{3} \\ \tilde{\phi}_f = 1 & \frac{2}{3} < \tilde{\phi}_B < 1 \\ \tilde{\phi}_f = \tilde{\phi}_B & \text{otherwise} \end{cases} \tag{26}$$

$$\text{Van Albada} \quad \begin{cases} \tilde{\phi}_f = \tilde{\phi}_B & \tilde{\phi}_B \leq 0 \text{ or } \tilde{\phi}_B \geq 1 \\ \tilde{\phi}_f = \tilde{\phi}_B + \frac{\tilde{\phi}_B(1-\tilde{\phi}_B)}{2-4\tilde{\phi}_B+4\tilde{\phi}_B^2} & 0 < \tilde{\phi}_B < 1 \end{cases} \tag{27}$$

It is obvious that with the use of the limiting functions, the programming becomes much easier and more efficient because those IF statements, as required in the NVF, become unnecessary.

Mass Fluxes

In our calculations, all variables are stored at the centroid of each control volume. It is known that with the collocated grid arrangement, checkerboard oscillations may arise in the solution due to the decoupling between the velocities and pressure on the same node. To avoid this problem, the velocities on the face are estimated by

$$\vec{V}_f = \overline{\vec{V}_f} - D_f(\nabla P_f - \overline{\nabla P}_f) \tag{28}$$

where

$$D_f = \left(\frac{\Delta V}{A_P}\right)_f = \frac{1}{2}\left[\left(\frac{\Delta V}{A_P}\right)_P + \left(\frac{\Delta V}{A_P}\right)_C\right] \tag{29}$$

Here A_P is the principal coefficient of the discretized momentum equation. The face values $\overline{\vec{V}_f}$ and $\overline{\nabla P}_f$ are obtained via interpolation from nodes P and C.

The mass flux across the face is then calculated in the following way:

$$\dot{m}_f = \rho_f \overline{\vec{V}_f} \bullet \vec{S}_f - \rho_f D_f (\nabla P_f - \overline{\nabla P_f}) \bullet \vec{d} = \rho_f \overline{\vec{V}_f} \vec{S}_f - B_C [(P_C - P_P) - \overline{\nabla P_f} \bullet \vec{\delta}_{PC}] \tag{30}$$

where

$$B_C = \rho_f D_f \frac{|\vec{S}_f|^2}{\vec{\delta}_{PC} \bullet \vec{S}_f} \tag{31}$$

In Eq. (30), term in brackets plays the role of a third-order correction to the mass flux.

In compressible flows, the density is a transport property governed by the continuity equation. Thus, the density on the face in calculating the mass flux is also calculated using the flux-limiter method shown by Eq. (17).

CHARACTERISTIC-BASED LIMITERS

In calculating the convective flux, as given in Eq. (17), the antidiffusion term is based on the primitive variables. In the following, we will show how to determine this antidiffusion term from characteristic variables. Let ϕ^l be the primitive variables (i.e., ρ, u, v, and e) and T_{lm} and T_{lm}^{-1} be the matrices, given by Eq. (7), to form the similarity transformation. The characteristic variables are then defined as

$$\varphi^l = T_{lm}^{-1} \phi^m \tag{32}$$

Multiplying Eq. (17) by T_{lm}^{-1} yields

$$\varphi_f^m = \varphi_B^m + \frac{\gamma_f^m(r^m)}{2} \Delta\varphi^m \tag{33}$$

where

$$\Delta\varphi^m = \varphi_D^m - \varphi_B^m \tag{34}$$

The gradient ratio r^m is now based on characteristic variables:

$$r^m \equiv \frac{\varphi_B^m - \varphi_U^m}{\varphi_D^m - \varphi_B^m} \tag{35}$$

Equation (33) is then multiplied by T_{lm} to convert the characteristic variables back to primitive variables to yield

$$\phi_f^l = \phi_B^l + \frac{1}{2} \sum_m \gamma_f^m(r^m) T_{lm} \Delta\varphi^m \tag{36}$$

where the summation is taken over the four characteristic variables.

To implement the above method, there are different ways to determine the characteristic variables at nodes D, B, and U, which may have a great effect on the solution. In one method, the characteristic variables are determined from

$$\varphi_D = T_B^{-1}\phi_D \qquad \varphi_B = T_B^{-1}\phi_B \qquad \varphi_U = T_B^{-1}\phi_U \tag{37}$$

where the matrix T^{-1} at the upstream node B is used in the determination of φ_D, φ_B, and φ_U. This approach is termed method 1 in the following. It is easy from Eq. (32) to show the characteristic variables in the following form:

$$\varphi^1 = \begin{bmatrix} (\gamma-2)\rho/\gamma \\ (k_2 u - k_1 v)/k^2 \\ k_1 u/2k + k_2 v/2k + c/\gamma \\ -(k_1 u/2k + k_2 v/2k) + c/\gamma \end{bmatrix} \tag{38}$$

Thus, an alternative approach, termed method 2, is to use the primitive variables directly at nodes D, B, and U to find the above characteristic variables at these nodes.

In characteristic variables, the two constants k_1 and k_2 need to be specified. In one method, these constants can be the directional cosines of the normal vector of the considered face. With this approach the characteristic variables need to be recalculated at each face in a cell. Another method is to use a unified direction. The direction of local pressure gradient in cell B is a suitable choice. This way is more economical in terms of computing time and is adopted in the following.

It is noted that instabilities may arise in some flow problems and prevent the solution procedure from converging. To suppress the instability, the convective flux needs to be further limited to introduce more diffusion into the scheme. This is achieved by limiting the limiter to a value less than 1, as will be discussed in the case of a NACA airfoil in the tests. It is noted that a value of γ_f smaller than 1 indicates that the scheme is biased toward the upwind direction, whereas for γ_f greater than 1 it becomes toward the downwind direction.

GRADIENT CALCULATIONS

As seen above, the gradients of variables need to be determined before calculating the diffusive and mass fluxes. Moreover, in determining the flux-limiting function, the far-upwind value φ_U depends on the gradient in the considered cell. The method used to estimate the gradient has significant effects on the accuracy. A simple approach to calculate the gradient is to use the discretized Gauss theorem.

$$\nabla\phi = \frac{1}{\Delta V}\sum \phi_f \vec{S}_f \tag{39}$$

where summation is over the surrounded faces of the control volume. The face value may be obtained from a simple interpolation from the two nodes sharing the same

face:

$$\phi_f = w\phi_C + (1-w)\phi_P \tag{40}$$

where w is a weighting factor.

The above linear interpolation approach is generally regarded as low-order-accurate in the gradient calculation because only the nearest neighbors are involved. For high-order accuracy, more neighboring nodes need to be included [17, 18, 28]. A second-order-accurate approach is based on a linear reconstruction of the solution in the cell to obtain the face value as [29]

$$\phi_f = \frac{1}{2}\left[(\phi_P + \nabla\phi_P^{(1)} \cdot \vec{\delta}_{Pf}) + (\phi_C + \nabla\phi_C^{(1)} \cdot \vec{\delta}_{Cf})\right] \tag{41}$$

where $\vec{\delta}_{Pf}$ and $\vec{\delta}_{Cf}$ are the distance vectors directed from node P and node C to face f, respectively. The gradients $\nabla\phi^{(1)}$ are obtained using the simple interpolation approach [Eq. (40)] for $\phi_f^{(1)}$. The resulting ϕ_f may not be bounded and may become greater than the nodal values surrounding the considered cell, which may lead to serious overshoots or undershoots in the region with a large change of gradient. Thus, the following limitation is imposed:

$$\phi_f = \min\left[\max(\min\{\phi_C\}, \phi_f), \max\{\phi_C\}\right] \tag{42}$$

where $\{\phi_C\}$ is a set consisting of all the values of the considered node and the nearest neighbors.

SOLUTION ALGORITHM

Adopted from the SIMPLE algorithm, the transport equations for the momentum and energy together with the continuity equation are solved sequentially in an iterative manner. The procedure consists of predictor and corrector steps in each iteration. In the predictor step the momentum equation is solved for the velocity $\vec{V}^*$ using the old Spressure field. The velocity and the pressure are then adjusted in the corrector step such that the continuity constraint is satisfied. The continuity equation can be discretized as

$$\rho' \frac{\Delta V}{\Delta t} + \sum_f \dot{m}_f = 0 \tag{43}$$

Here the mass flux can be expressed as

$$\dot{m}_f = \dot{m}_f^* + \dot{m}_f' = \rho_f^* \vec{V}_f^* \cdot \vec{S}_f + (\rho_f^* \vec{V}_f' + \rho_f' \vec{V}_f^*) \cdot \vec{S}_f \tag{44}$$

where the superscripts * denote the prevailing values, and the superscripts the corrections. The velocity and density corrections can be related to the pressure

correction by

$$\vec{V}'_f = -D_f \nabla P'_f \tag{45}$$

$$\rho' = KP' \tag{46}$$

Thus,

$$\dot{m}'_f = -\rho^*_f D_f \nabla P'_f \cdot \vec{S}_f + \frac{\dot{m}^*_f}{\rho^*_f} K_f P'_f \tag{47}$$

In this equation, the first term represents the diffusion of P' and the second term stands for the convection. In incompreesible flows, the convection term does not exist. The ratio the coefficients of the two terms is a function of Mach number. At high Mach number, the convection becomes dominant and the expression behaves in a hyperbolic manner. Using the same treatment described above for the convective and diffusive fluxes [Eqs. (15) and (17)], the mass flux correction can be written as

$$\begin{aligned}\dot{m}'_f = {} & B_C(P'_P - P'_C) - \rho^*_f D_f \overline{\nabla P}'_f \cdot (\vec{S}_f - \vec{d}) \\ & + \max\left(\frac{\dot{m}^*_f}{\rho^*_f}, 0\right)\left[K_P P'_P + \frac{\gamma_f(r)}{2}(K_C P'_C - K_P P'_P)\right] \\ & + \min\left(\frac{\dot{m}^*_f}{\rho^*_f}, 0\right)\left[K_C P'_C + \frac{\gamma_f(r)}{2}(K_P P'_P - K_C P'_C)\right]\end{aligned} \tag{48}$$

Introduction into Eq. (43) results in an equation for P'

$$A_P P'_P = \sum_C A_C P'_C + S \tag{49}$$

The coefficients A_C take the form

$$A_C = B_C - \min\left(\frac{\dot{m}^*_f}{\rho^*_f}, 0\right) K_C \tag{50}$$

It is noted that the cross-derivative term of the diffusive flux and the antidiffusion term of the convective flux are absorbed into the source S. They can be taken into account by solving the pressure-correction equation in a predictor-corrector way [24, 25].

The solution procedure is to solve the momentum equation first to obtain a predicting velocity field. This followed by solving the pressure-correction equation. In this step, the velocities and pressure are updated using the resulting pressure corrections. Finally, the temperature field is found by solving the energy equation. The new density is then obtained according to the equation of state. This completes a

time step (or an iteration). The same procedure is repeated until the solution converges.

VALIDATION OF THE ALGORITHM

Three different flow configurations are considered to validate the above solution procedure and to assess its accuracy. The first is the quasi-one-dimensional flow in a convergent-divergent nozzle, which serves as a valuable benchmark because the theoretical solution exists. Another test case is the trans-sonic flow over a NACA 0012 airfoil. The last test case is the flow through a double-throat nozzle in which the Mach number at the outlet can be as high as 2.0. Reference data are available for the last two flows, which have been selected as test cases in the GAMM Workshop [30], among others.

In the following calculations, two difference schemes (the Van Albada scheme and the SUPERBEE scheme), two different approaches for the characteristic-based limiters (the matrix transformation approach, denoted method 1, and the direct use of characteristic variables, denoted method 2), and two different ways for gradient calculations (the linear-interpolation method and the linear-reconstruction method) are applied. In addition, the limiters based on primitive variables are also incorporated for comparison. Convergence of the solution iteration is based on the L1 norm of the residuals of the discretized momentum and pressure-correction equations normalized by the corresponding intake fluxes.

Convergent-Divergent Nozzle

The inviscid flow in a convergent-divergent nozzle has been considered by the present authors as a benchmark test problem [24]. The theoretical solution can be obtained from one-dimensional gas dynamics theory. The variation of the cross-sectional area of the considered nozzle is given by

$$S(x) = 1 + \left(1 - \frac{x}{5}\right)^2 \qquad 0 \le x \le 10 \tag{51}$$

For back pressures of 0.87 Po, 0.769 Po, and 0.645 Po (Po being the stagnation pressure) a normal shock stands at locations $x = 7$, 8, and 9, respectively. The following calculations are performed on a 200×20 grid. It is seen from Figure 3*a* that, comparing with the Van Albada limiter, the SUPERBEE limiter gives rise to a sharper gradient in the shock region, but the oscillations behind the shock become more serious. It is generally recognized that among a variety of TVD schemes the SUPERBEE limiter is less diffusive and more compressive [31]. By shifting the characteristic-based method 1 to method 2, the oscillating phenomenon is soothed, but the shocks become more smeared. In the above computations, the gradients are calculated using face values obtained from the simple interpolation of Eq. (40). The use of the high-order linear-reconstruction approach, as given by Eq. (41), gives rise to the results shown in Figure 3*b*. Comparing with Figure 3*a*, it is revealed that the strengths of the oscillations are reduced, especially by method 2 along with the Van Albada limiter. Another obvious benefit is that the smear of the shock becomes less

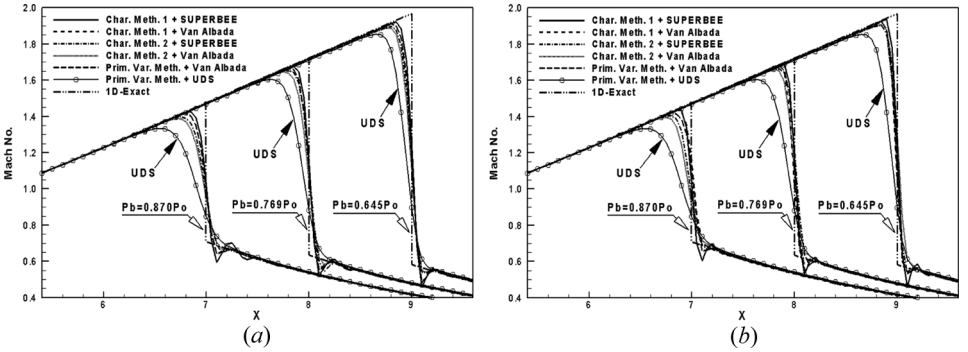

Figure 3. Variation of the Mach number along the centerline of the convergent-divergent nozzle.

prominent. The Van Albada limiter based on primitive variables is adopted in computations as well. It leads to results similar to those obtained by the characteristic-based method 1. The results for the first-order upwind difference scheme (UDS) are also shown in the figures. As expected, the UDS results in serious smear in the shock region. In the following, unless otherwise stated, the results obtained using the SUPERBEE limiter and the linear-reconstruction method for gradient calculations are presented.

NACA 0012 Airfoil

The flow past a NACA 0012 airfoil has been chosen as a test problem for evaluation of numerical schemes by numerous researchers [28, 30, 32]. In the following, we consider (1) the inviscid flow with free-stream Mach number $M_\infty = 0.80$ and angle of attack $\alpha = 1.25^\circ$, and (2) the viscous flow with $M_\infty = 0.80$, $\alpha = 10.0^\circ$, and Reynolds number $\mathrm{Re}_\infty = 500$. As seen from Figure 4, the grid adopted is of O type

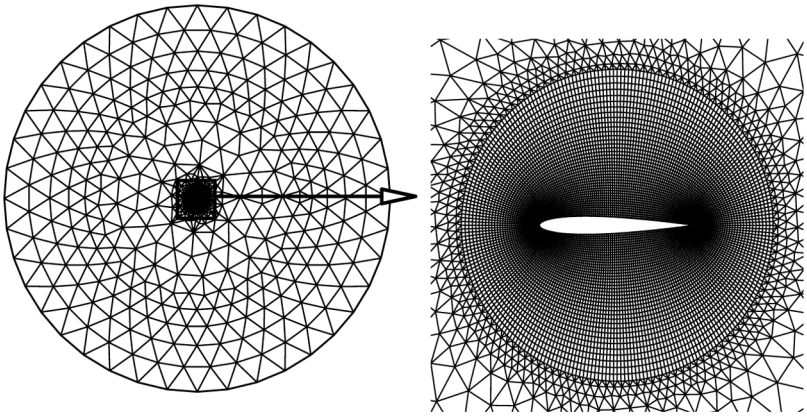

Figure 4. Computational grid for the NACA 0012 airfoil.

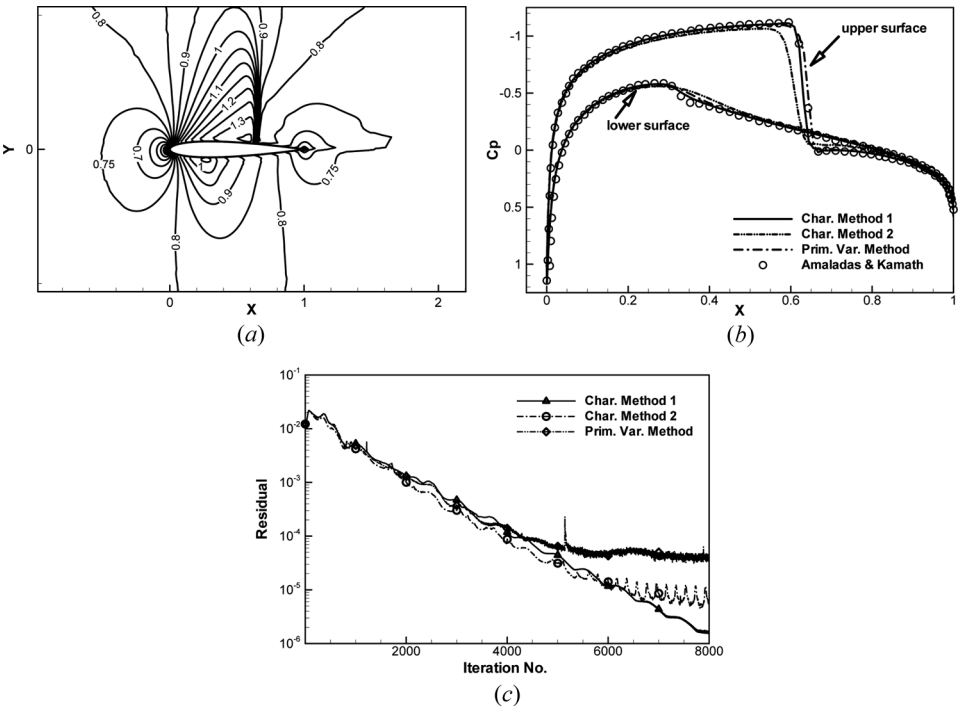

Figure 5. Inviscid flow past the NACA 0012 airfoil with $M_\infty = 0.80$ and $\alpha = 1.25^\circ$: (*a*) Mach contours; (*b*) pressure coefficient along the airfoil surfaces; (*c*) convergence history.

with 256 nodes on the surface of the airfoil. There are 256×40 quadrilateral cells in the field near the airfoil and 1,062 triangular cells in the far field. The results for the inviscid and viscous flows are shown in Figures 5 and 6, respectively. The Mach contours shown in Figure 5*a* for the inviscid flow indicate that a strong shock appears on the upper surface. The distribution of pressure coefficient on the upper surface given in Figure 5*b* implies good shock-capturing capability of the present methods. It can be seen that a slight undershoot is detected in the solution just behind the shock for the calculations using the primitive variable–based limiter. With the characteristic-based methods this phenomenon diminishes. The capture of the position and the strength of the shock by the characteristic-based method 1 agrees well with the predictions of Amaladas and Kamath [32]. The shock is moved slightly forward and becomes smeared using method 2. On the lower surface of the airfoil, the predictions of Amaladas and Kamath [32] indicate the existence of a weak shock, which can also be identified in the calculations by method 1, but is nearly smeared out by method 2 and the primitive variable-based method.

Comparison of the convergence histories of the pressure-correction equation for the consider methods is shown in Figure 5*c*. With the primitive variable-based method the residual levels off early. The residuals for the two characteristic-based methods can be reduced to lower values, with method 1 being slightly more effective in this case.

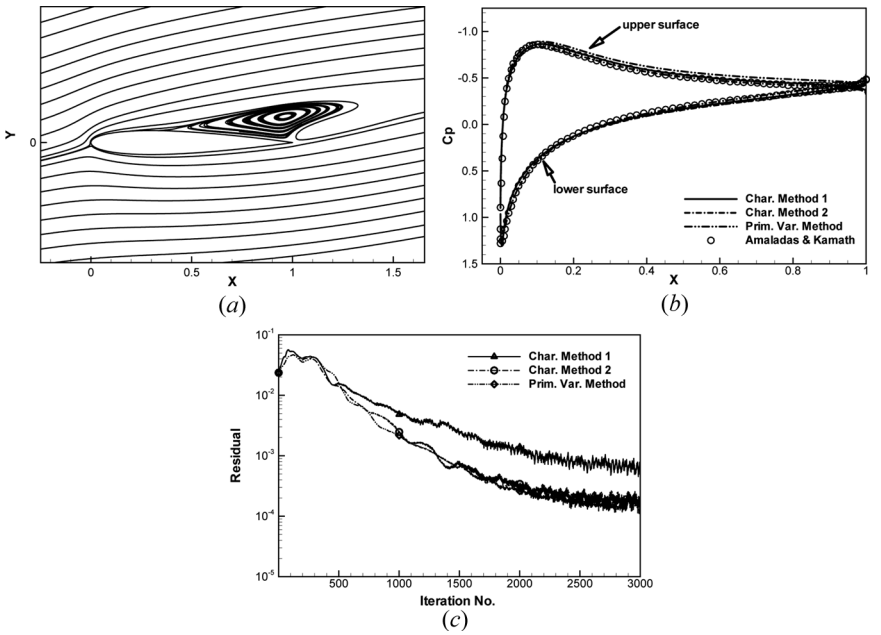

Figure 6. Viscous flow past the NACA 0012 airfoil with $M_\infty = 0.80$, $\alpha = 10.0^\circ$, and $\mathrm{Re}_\infty = 500$: (*a*) Mach contours; (*b*) pressure coefficient along the airfoil surfaces; (*c*) convergence history.

The most prominent feature of the viscous flow past the airfoil at an angle of attack of 10° and a Reynolds number of 500 is the presence of a large separation region on the upper surface, covering more than half of the chord, as seen in Figure 6*a*. The predicted pressure distribution over the upper and lower surfaces shown in Figure 6*b* is similar to that reported by Jawahar and Kamath [28]. No shock wave is generated on the airfoil surface in the viscous flow. The pressure coefficient is a little too low on the upper surface predicted by the primitive variable–based method. It is revealed from the convergence history shown in Figure 6*c* that the curves for the characteristic-based method 1 tend to level off more quickly than those for the characteristic-based method 2 and the primitive variable–based method.

The appearance of the strong shock in the inviscid flow and the large separation bubble in the viscous flow causes difficulty for the methods, especially the characteristic-based method 1 and the primitive variable–based method, to converge. The instabilities, in most flow calculations, can be suppressed by the characteristic-based method 2 because of its dissipative nature. To introduce dissipation into the solution procedure, a maximum value less than 1 must be imposed on the limiters in the other two methods. For the characteristic-based method 1, a maximum value of 0.9 is assigned to all the characteristic-based limiters in the above calculations. As for the primitive variable–based method, limitation is imposed on the limiter for the density only [24]. A value of 0.4 is used for the inviscid flow and a value of 0.2 for the viscous flow. It is noted that as the maximum restrictive value becomes lower, the higher is the dissipation and, usually, the faster is the convergence rate. This explains why the characteristic-based method 2 does not always converge faster than the

other methods. The results shown above were obtained using the SEPERBEE limiter. It was found that by changing to the Van Albada limiter, the shock becomes more smeared and the convergence rate is faster. This is not unexpected because of its higher dissipation.

Double-Throat Nozzle

The viscous flow in a double-throat nozzle is used as a validation case for high-speed-flow calculations. The compression waves in the region between the two throats may cause separation, which makes this flow suitable to test the shock wave/boundary-layer interaction. This flow problem also appeared in the GAMM Workshop as a benchmark test case [30]. At the inlet, total pressure and total temperature are specified, while extrapolations are undertaken for all variables at the outlet. In addition, extrapolation is also used for the horizontal velocity component at the inlet. On the solid wall, no-slip condition is imposed and the temperature is set at the total temperature. The Reynolds numbers considered are 100, 400, and 1,600. The grid used contains 315×40 quadrilateral cells with dense meshes in the region near the wall. A grid layout (157×20) is illustrated in Figure 7.

The Mach contours in an increment $\Delta M = 0.2$ are shown in Figure 8. The iso-Mach lines with Mach numbers 1 and 2 are marked in the plots. For the flow with the lowest Reynolds number the viscous effects is more obvious; the subsonic flow covers one-fourth of the outlet region. The flow separates from the wall in the divergent part of the first throat to form a bubble. When the Reynolds number is increased to 400, the extent of the subsonic region is reduced and a normal shock is formed at about $x = 5$. For the highest Reynolds number, the separation bubble becomes much thinner due to the reduction of the boundary-layer thickness. A weak oblique shock wave can be identified in the region between $x = 3$ and $x = 6$, followed by a stronger shock wave reflected from the centerline. A second separation bubble can be found near the second throat, due to the interaction between the reflected shock wave and the viscous layer. The resulting separation points X_s and the reattachment points X_r obtained using the two characteristic-based methods and the two limiters for the three cases are shown in Table 1. They agree well with the data provided by various researchers at the GAMM Workshop. The distributions of

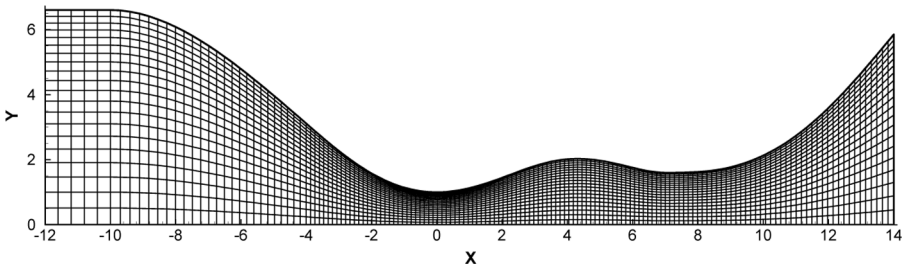

Figure 7. A typical grid for the double-throat nozzle.

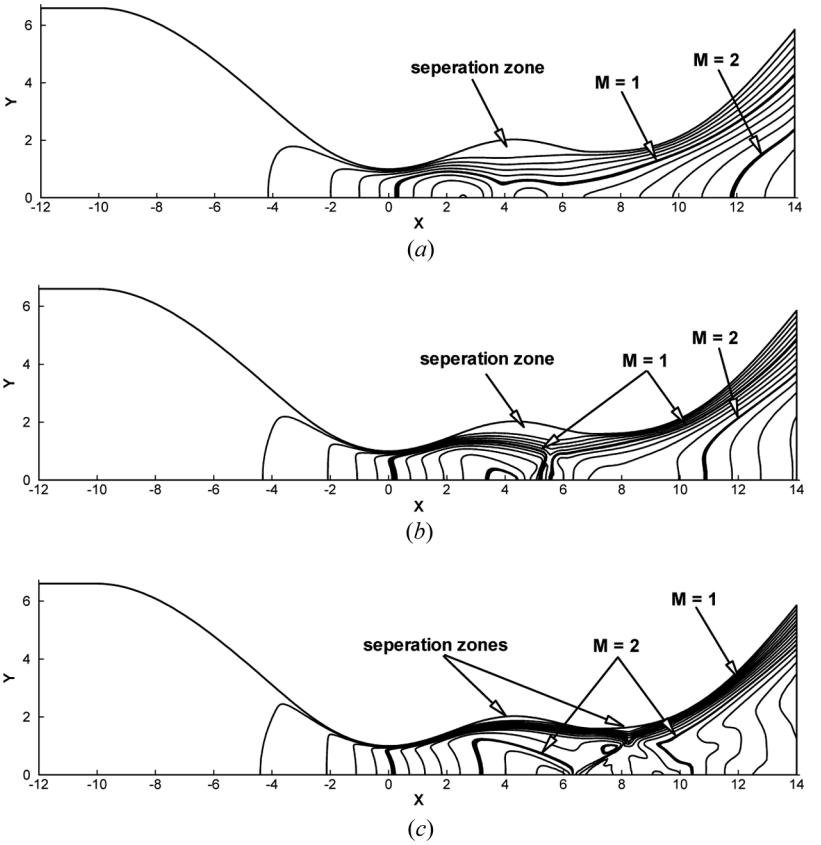

Figure 8. Distribution of Mach number for the flow through the double-throat nozzle at (*a*) $\mathrm{Re_o} = 100$, (*b*) $\mathrm{Re_o} = 400$, and (*c*) $\mathrm{Re_o} = 1600$. The contour lines are plotted in an increment of 0.2.

the Mach number and the pressure along the centerline as well as the skin friction coefficient along the wall are given in Figure 9. Comparison with a number of computational results provided at the GAMM Workshop at some selected points validates the present calculations.

Table 1. Separation and reattachment points of the separation zones

Authors	$\mathrm{Re_o} = 100$ X_s/X_r	$\mathrm{Re_o} = 400$ X_s/X_r	$\mathrm{Re_o} = 1600$ X_{s_1}/X_{r_1}	$\mathrm{Re_o} = 1600$ X_{s_2}/X_{r_2}
Char. method1 + Van Albada	3.024/4.811	2.995/6.245	3.429/4.708	8.114/8.322
Char. method1 + SUPERBEE	3.024/4.802	2.976/6.183	3.429/4.703	8.091/8.317
Char. method2 + Van Albada	3.038/4.802	3.032/6.277	3.422/4.674	8.122/8.227
Char. method2 + Van Albada	3.041/4.803	2.992/6.257	3.406/4.669	8.046/8.248
GAMM Workshop [30]	2.951–3.004/ 4.811–4.848	2.962–3.005/ 6.188–6.241	3.424–3.438/ 4.688–4.739	8.006–8.077/ 8.188–8.280

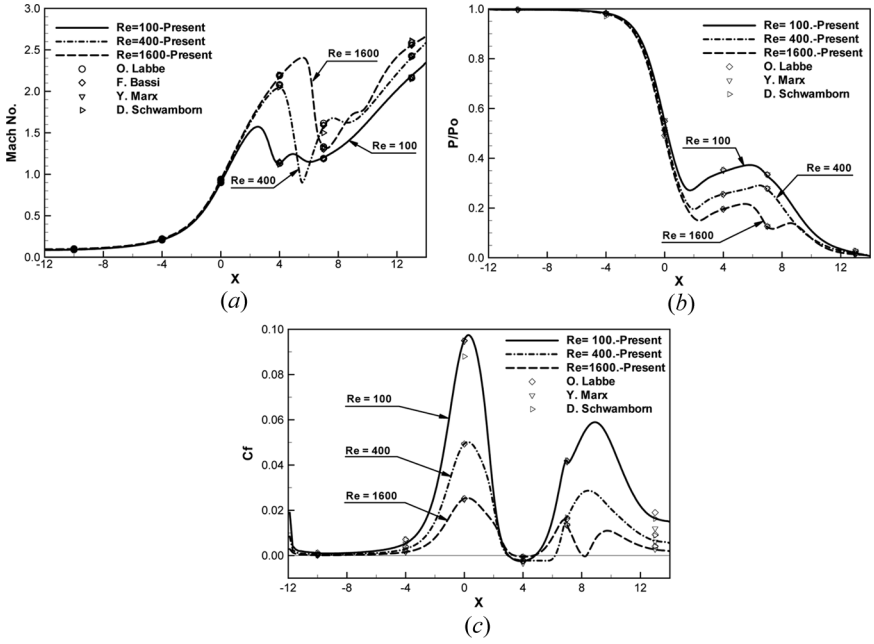

Figure 9. The case of flow through the double-throat nozzle: (*a*) variation of Mach number along the centerline; (*b*) variation of pressure along the centerline; (*c*) variation of skin friction coefficient along the wall.

CONCLUSIONS

A solution method, based on the pressure-correction approach and suited to all flows ranging from incompressible to compressible, has been developed and tested. It features the use of unstructured meshes and is applicable to flow fields with extremely complicated geometry. To obtain high resolution in the region with large variation of gradient, either the TVD scheme or the NVD scheme can easily be implemented to limit the convective flux. The determination of the flux limiter is based on the use of characteristic variables. Two different approaches have been proposed to determine the characteristic variables in determining the flux limiters: the matrix transformation method (method 1) and the direct method (method 2). It has been shown in the test cases that satisfactory results in the regions near the shock and the solid wall are obtained. However, the wiggles in the shock region cannot be completely eliminated, especially by method 1. This situation is alleviated with the use of method 2, but at the cost of slight smear of the shock wave. This result implies that method 2 has slightly higher numerical dissipation. A further demonstration can be seen in the flow past the NACA airfoil. With method 2, in general, there is no need to restrict the flux limiter in most flow calculations, whereas a maximum value less than 1 must be imposed on the limiter when method 1 or the primitive variable–based method is used. Comparing with the primitive variable–based method, an advantage of using the characteristic-based methods is the fast convergence rate. This is especially true for method 2. It was seen that by using method 2, the residual can be reduced to a small value without causing levelling off of the convergence curve too quickly.

REFERENCES

1. Y.-Y. Tsui, A Study of Upstream-Weighted High-Order Differencing for Approximation to Flow Convection, *Int. J. Numer. Meth. Fluids*, vol. 13, pp. 167–199, 1991.
2. D. B. Spalding, A Novel Finite Difference Formulation for Differential Expression Involving Both First and Second Derivatives, *Int. J. Numer. Meth. Eng.*, vol. 4, pp. 551–559, 1972.
3. J. P. Borris and D. L. Brook, Flux-Corrected Transport I: SHASTA, A Fluid Transport Algorithm That Works, *J. Comput. Phys.*, vol. 11, pp. 36–89, 1971.
4. R. M. Beam and R. F. Warming, An Implicit Finite-Difference Algorithm for Hyperbolic System in Conservation-Law Form, *J. Comput. Phys.*, vol. 22, pp. 87–110, 1976.
5. J. L. Steger and R. F. Warming, Flux Vector Splitting of the Inviscid Gasdynamic Equations with Application to Finite-Difference Methods, *J. Comput. Phys.*, vol. 40, pp. 263–293, 1981.
6. W. K. Anderson, J. L. Thomas, and B. Van Leer, Comparison of Finite Volume Flux Vector Splitting for the Euler Equations, *AIAA J.*, vol. 24, pp. 1453–1460, 1986.
7. A. Harten, High Resolution Schemes for Hyperbolic Conservation Laws, *J. Comput. Phys.*, vol. 49, pp. 357–393, 1983.
8. P. K. Sweby, High Resolution Schemes Using Flux Limiters for Hyperbolic Conservation Laws, *SIAM J. Numer. Anal.*, vol. 21, pp. 995–1011, 1984.
9. S. R. Chakravarthy and S. Osher, High Resolution Application of the OSHER Upwind Scheme for the Euler Equations, AIAA Paper 83–1943, 1983.
10. B. P. Leonard, Simple High-Accuracy Resolution Program for Convective Modeling of Discontinuities, *Int. J. Numer. Meth. Fluids*, vol. 8, pp. 1291–1318, 1988.
11. P. H. Gaskell and A. K. C. Lau, Curvature-Compensated Convective Transport: SMART, A New Boundedness-Preserving Transport Algorithm, *Int. J. Numer. Meth. Fluids*, vol. 8, pp. 617–641, 1988.
12. B. P. Leonard, The ULTIMATE Conservative Difference Scheme Applied to Unsteady One-Dimensional Advection, *Comput. Meth. Appl. Mech. Eng.*, vol. 88, pp. 17–74, 1991.
13. W. A. Mulder and B. Van Leer, Experiments with Implicit Upwind Methods for the Euler Equations, *J. Comput. Phys.*, vol. 59, pp. 232–246, 1985.
14. G. D. Van Albada, B. Van Leer, and W. W. Roberts, Jr., A Comparative Study of Computational Methods in Cosmic Gas Dynamics, *Astron. Astrophys.*, vol. 108, pp. 76–84, 1982.
15. H. Lin and C.-C. Chieng, Characteristic-Based Flux Limiters of an Essentially Third-Order Flux-Splitting Method for Hyperbolic Conservation Laws, *Int. J. Numer. Meth. Fluids*, vol. 13, pp. 287–307, 1991.
16. A. Dadone and B. Grossman, Characteristic-Based, Rotated Upwind Scheme for the Euler Equations, *AIAA J.*, vol. 30, pp. 2219–2226, 1992.
17. D. Pan and J.-C. Cheng, A Second-Order Upwind Finite-Volume Method for the Euler Solution on Unstructured Triangular Meshes, *Int. J. Numer. Meth. Fluids*, vol. 16, pp. 1079–1098, 1993.
18. T. J. Barth and D. C. Jespersen, The Design and Application of Upwind Schemes on Unstructured Meshes, AIAA Paper 89–0366, 1989.
19. M. H. Kobayashi and J. C. F. Pereira, Characteristic-Based Pressure Correction at All Speeds, *AIAA J.*, vol. 34, pp. 272–280, 1996.
20. P. L. Roe, Approximate Riemann Solvers, Parameter Vectors and Difference Schemes, *J. Comput. Phys.*, vol. 43, pp. 357–372, 1981.
21. P. L. Roe, Characteristic-Based Schemes for the Euler Equations, *Ann. Rev. Fluid Mech.*, vol. 18, pp. 337–365, 1986.

22. R. I. Issa and M. H. Javareshkian, Pressure-Based Compressible Calculation Method Utilizing Total Variation Diminishing Schemes, *AIAA J.*, vol. 36, pp. 1652–1657, 1998.
23. H. C. Yee, R. F. Warming, and A. Harten, Implicit Total Variation Diminishing (TVD) Schemes for Steady-State Calculations, *J. Comput. Phys.*, vol. 57, pp. 327–360, 1985.
24. Y.-Y. Tsui and T.-C. Wu, A Pressure-Based Unstructured-Grid Algorithm Using High-Resolution Schemes for All-Speed Flows, *Numer. Heat Transfer B*, vol. 53, pp. 75–96, 2008.
25. Y.-Y. Tsui and Y.-F. Pan, A Pressure-Correction Method for Incompressible Flows Using Unstructured Meshes, *Numer. Heat Transfer B*, vol. 49, pp. 43–65, 2006.
26. P. L. Roe, Some Contributions to the Modeling of Discontinuous Flows, in E. Engquist et al. (eds.), *Large Scale Computations in Fluid Mechanics, Part 2* (Lectures in Applied Mathematics, vol. 22), pp. 163–193, American Mathematics Society, Providence, RI., 1985.
27. P. G. D. Van Albada, B. Van Leer, and W. W. Roberts, Jr., A Comparative Study of Computational Methods in Cosmic Gas Dynamics, *Astron. Astrophys.*, vol. 108, pp. 76–84, 1982.
28. P. Jawahar and H. Kamath, A High-Resolution Procedure for Euler and Navier-Stokes Computation on Unstructured Grids, *J. Comput. Phys.*, vol. 164, pp. 165–203, 2000.
29. S. R. Mathur and J. Y. Murthy, A Pressure-Based Method for Unstructured Meshes, *Numer. Heat Transfer B*, vol. 31, pp. 195–215, 1997.
30. M. O. Bristeau, R. Glowinski, J. Periaux and H. Viviand, Numerical Simulation of Compressible Navier-Stokes Flows, *Notes on Numer. Fluid Mech.*, vol. 18, Braunschweig; Wiesbaden, Vieweg, 1987.
31. Y. N. Jeng and U. J. Payne, An Adaptive TVD Limiter, *J. Comput. Phys.*, vol. 118, pp. 229–241, 1995.
32. J. R. Amaladas and H. Kamath, Accuracy Assessment of Upwind Algorithms for Steady-State Computations, *Comput. Fluids*, vol. 27, pp. 941–962, 1998.